\

Defect calculations with quasiparticle correction: A revisited study of iodine defects in $CH_3NH_3PbI_3$

Ling Li(李玲) and Wan-Jian Yin(尹万健)

Citation: Chin. Phys. B, 2022, 31 (**1**): 017103. DOI: 10.1088/1674-1056/ac3505
Journal homepage: http://cpb.iphy.ac.cn; http://iopscience.iop.org/cpb

What follows is a list of articles you may be interested in

First-principles study on improvement of two-dimensional hole gas concentration and confinement in AlN/GaN superlattices

Huihui He(何慧卉) and Shenyuan Yang(杨身园)
Chin. Phys. B, 2022, 31 (**1**): 017104. DOI: 10.1088/1674-1056/ac00a0

Magnetic and electronic properties of two-dimensional metal-organic frameworks $TM_3(C_2NH)_{12}$

Zhen Feng(冯振), Yi Li(李依), Yaqiang Ma(马亚强), Yipeng An(安义鹏), and Xianqi Dai(戴宪起)
Chin. Phys. B, 2021, 30 (**9**): 097102. DOI: 10.1088/1674-1056/ac0cdb

Passivation and dissociation of P_b-type defects at a-SiO_2/Si interface

Xue-Hua Liu(刘雪华), Wei-Feng Xie(谢伟锋), Yang Liu(刘杨), and Xu Zuo(左旭)
Chin. Phys. B, 2021, 30 (**9**): 097101. DOI: 10.1088/1674-1056/ac0e20

Bilayer twisting as a mean to isolate connected flat bands in a kagome lattice through Wigner crystallization

Jing Wu(吴静), Yue-E Xie(谢月娥), Ming-Xing Chen(陈明星), Jia-Ren Yuan(袁加仁), Xiao-Hong Yan(颜晓红), Sheng-Bai Zhang(张绳百), and Yuan-Ping Chen(陈元平)
Chin. Phys. B, 2021, 30 (**7**): 077104. DOI: 10.1088/1674-1056/abd7d6

Tunable bandgaps and flat bands in twisted bilayer biphenylene carbon

Ya-Bin Ma(马亚斌), Tao Ouyang(欧阳滔), Yuan-Ping Chen(陈元平), and Yue-E Xie(谢月娥)
Chin. Phys. B, 2021, 30 (**7**): 077103. DOI: 10.1088/1674-1056/ac009e

---

Defect calculations with quasiparticle correction: A revisited study of iodine defects in $CH_3NH_3PbI_3$

Ling Li(李玲)[1] and Wan-Jian Yin(尹万健)[1,2,3,†]

[1] *College of Energy, Soochow Institute for Energy and Materials Innovations (SIEMIS), and Jiangsu Provincial Key Laboratory for Advanced Carbon Materials and Wearable Energy Technologies, Soochow University, Suzhou* 215006, *China*

[2] *Light Industry Institute of Electrochemical Power Sources, Soochow University, Suzhou* 215006, *China*

[3] *Key Laboratory of Advanced Optical Manufacturing Technologies of Jiangsu Province & Key Laboratory of Modern Optical Technologies of the Education Ministry of China, Soochow University, Suzhou* 215006, *China*

(Received 23 August 2021; revised manuscript received 14 October 2021; accepted manuscript online 1 November 2021)

Defect levels in semiconductor band gaps play a crucial role in functionalized semiconductors for practical applications in optoelectronics; however, first-principle defect calculations based on exchange–correlation functionals, such as local density approximation, grand gradient approximation (GGA), and hybrid functionals, either underestimate band gaps or misplace defect levels. In this study, we revisited iodine defects in $CH_3NH_3PbI_3$ by combining the accuracy of total energy calculations of GGA and single-electron level calculation of the GW method. The combined approach predicted neutral I_i to be unstable and the transition level of $I_i(+1/-1)$ to be close to the valence band maximum. Therefore, I_i may not be as detrimental as previously reported. Moreover, V_I may be unstable in the -1 charged state but could still be detrimental owing to the deep transition level of $V_I(+1/0)$. These results could facilitate the further understanding of the intrinsic point defect and defect passivation observed in $CH_3NH_3PbI_3$.

Keywords: quasiparticle correction, defect calculation, GW theory, methylammonium lead iodide

PACS: 71.15.Mb, 61.72.Bb, 31.15.xm **DOI:** 10.1088/1674-1056/ac3505

1. Introduction

As crucial features in functional semiconductors, defect properties, typically as defect formation and transition energies, are generally calculated using the first-principle density-functional theory (DFT) based on different approximations of exchange–correlation functionals such as local density approximation (LDA), grand gradient approximation (GGA), and hybrid functionals.[1–10] DFT based on LDA/GGA is known to be reliable for calculating the total energies of a bulk system that is free of defect states.[11–14] However, owing to the existence of artificial self-interaction and the absence of the derivative discontinuity in the exchange–correlation potential, DFT-LDA/GGA does not accurately estimate the electronic eigenvalues, resulting in the underestimation of the band gap and inaccurate positioning of the single-electron defect level.[2,15–18] Although the hybrid functional method can reproduce the experimental band gap, it is, to some extent, still an empirical approach, as the exact exchange portion is an empirical parameter.[2,19,20] In addition, its reliability in calculating the position of defect states has been challenged.[2,5,19,21] The GW approach, based on the many-body perturbation theory applied to Green's function, provides a more rigorous theoretical framework for the improvement of the estimation accuracy of a band gap and single-electron level.[22,23] However, owing to the heavy computational cost, the total energy calculations, and thus atomic relaxations, have not been effectively implemented within the framework of the GW method.[24,25]

In this work, we combined the total energy calculation at the DFT level with the single-electron level calculation of the GW method to improve the accuracy of defect calculations. As a case study, we applied this approach to investigate iodine vacancies and iodine interstitials in $CH_3NH_3PbI_3$, a class of prevalent defects existing in an emerging perovskites solar cell, which are believed to be responsible for the nonradiative recombination of photoexcited carriers.[26] Recent DFT calculations have yielded scattered results for the transition levels of V_I and I_i,[9,27–31] as shown in Fig. 1. For example, V_I was initially considered to introduce shallow defect levels, with a transition level at the conduction band minimum of (CBM)+0.01 eV.[9] In contrast to conventional models where V_I is a donor, in this study, V_I was able to acquire an additional electron, attained a stable dimer structure, and obtained a deep transition level below the CBM.[30]

Defect calculations via PBE, PBE-SOC, and hybrid functional plus spin–orbit coupling (HSE-SOC) have also been performed for comparison with GW-SOC approaches. It has been found that GW-SOC generally pulls down the single-electron level for the occupied state and pushes up the single-electron level for the unoccupied state. The GW-SOC approach predicted neutral I_i to be unstable and that the transition level of $I_i(+1/-1)$ is close to the valence band maximum (VBM), therefore, the level of I_i may not be as detrimental as previously reported. GW-SOC calculations additionally showed that V_I may be unstable in the -1 charged state, in contrast to previous reports, but could still be detrimental due to the deep transition level of $V_I(+1/0)$. GW results are con-

†Corresponding author. E-mail: wjyin@suda.edu.cn

sistent with the experiment reporting a shallow donor level close to the CBM.[32] These results help further understand the intrinsic point defect and defect passivation observed in $CH_3NH_3PbI_3$.

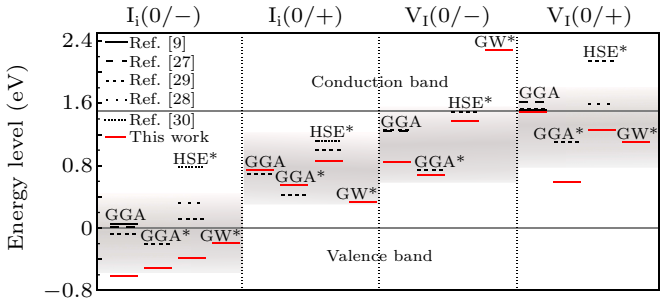

Fig. 1. Transition levels of V_I and I_i were reported in the literatures and this work. For ease of comparison, we unified the band gap to 1.5 eV. The red line represents the data of this work. The star $*$ indicates that the SOC effect was considered. The rendering band represents the approximate position range of the iodine defect charge transition energy level in the band gap obtained by combining all the current data work.

2. Calculation methods

We performed first-principles calculations based on the density functional theory (DFT) implemented in the VASP program. The electron–ion interactions were described by projector augmented wave (PAW) potentials. The generalized gradient approximation (GGA) of PBE, HSE, and the quasi-particle GW method was used as exchange–correlation functionals. β-$CH_3NH_3PbI_3$ was used to study the native iodine defect. The PBE method was used to optimize the lattice constants ($a = 8.69$ Å and $c = 12.66$ Å) of the bulk structure. The $2 \times 2 \times 1$ supercell structure and the subsequent defect structure were constructed based on this structure. The valence wave function was extended based on the plane wave sets with an energy cutoff of 300 eV. All atoms were relaxed to minimize the Hellmann–Feynman force to less than 0.01 eV /Å. An identical convergence standard was used at all calculation levels. Only Γ point was considered as the k-point sampling in the Brillouin zone in defect calculation.

3. Results and discussion

3.1. GW-correction on single-electron levels

Defect calculations based on first-principles calculations are often performed on a mixed scheme to combine the advantage of the special k-point and Γ point-only approaches.[23] The formation energy based on DFT-PBE calculations is accordingly given by

$$\begin{aligned}\Delta H_{\rm f}^{\rm PBE}(\alpha,q) = {} & \Delta H_{\rm f}^{\rm PBE}(\alpha,0) \\ & + \left[E^{\rm PBE}(\alpha,q) - \left(E^{\rm PBE}(\alpha,0) - q\varepsilon_{\rm D}^{k}(0)\right)\right] \\ & - q\left[\varepsilon_{\rm D}^{\tau}(0) - \varepsilon_{\rm VBM}^{\tau}({\rm host})\right] + qE_{\rm F}^{\rm PBE}, \end{aligned} \quad (1)$$

where the first two terms are related to total energies and the third term is concerning the single-electron energy level. In our approach, the total energy term and single-electron energy level were calculated with the PBE and GW-SOC approaches, respectively.

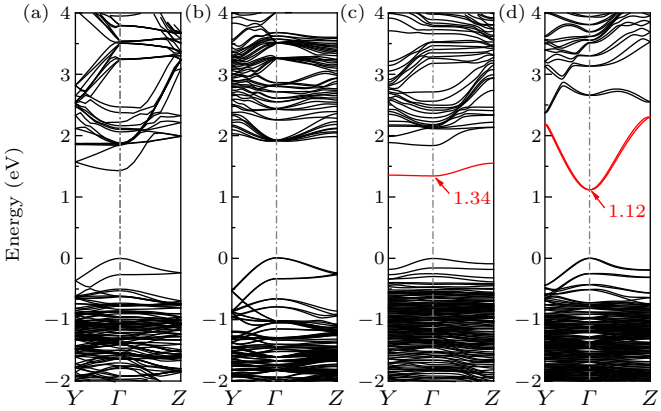

Fig. 2. Band structure of bulk $CH_3NH_3PbI_3$ obtained through the (a) PBE calculation and (b) GW-SOC calculation. Band structure of defective $CH_3NH_3PbI_3$ with V_I^1 (dimer structure) obtained through the (c) PBE calculation and (d) GW-SOC calculation. The red lines indicate the defect band.

To demonstrate how the GW correction on single-electron level calculation is performed, we took defective $CH_3NH_3PbI_3$ (with V_I^{1-}) as an example and show its band structure together with that of crystal $CH_3NH_3PbI_3$ under PBE and GW-SOC calculations in Fig. 2. The SOC was added due to the strong SOC effect observed in heavy Pb atoms.[33] As shown in the figure, PBE resulted in a proper band gap of 1.43 eV, close to the experimental value,[34] owing to the occasional cancellation of PBE underestimation and non-SOC overestimation. GW-SOC yielded a band gap of 1.90 eV, a little larger than the experimental band gap, probably due to the nonconvergent initialization, perhaps of the energy cutoff (a larger cutoff is computationally too heavy for defective calculations). GW corrections on defect calculations rely on the term $\varepsilon_{\rm D}^{\tau}(0) - \varepsilon_{\rm VBM}({\rm host})$, namely, the single-electron energy level at the Γ point referred to the VBM. Taking V_I^{1-} for example, the defect bands are marked red as shown in Fig. 2 and the values of $\varepsilon_{\rm D}^{\tau}(0) - \varepsilon_{\rm VBM}({\rm host})$ are shown accordingly. The value of the GW correction was then scaled according to the $[\varepsilon_{\rm D}^{\tau}(0) - \varepsilon_{\rm VBM}({\rm host})]E_{\rm g}^{\rm PBE}/E_{\rm g}^{\rm GW}$, as shown in Fig. 3. In addition, the figure shows the GW corrections of single-electron energy levels for all other defects.

We have found that in general, in comparison to PBE calculations, GW-SOC will pull down the energy level for an occupied state and push up the energy level for an unoccupied state. For example, the single-electron level of I_i^0 is occupied by one electron and located at the VBM $+0.50$ eV in the PBE calculation. In GW-SOC, this level was moved closer to the VBM, sitting at VBM $+0.09$ eV. In contrast, the single-electron level of I_i^+ is empty and located at the CBM -0.27 eV in the PBE calculation. In GW-SOC, this level moved above the CBM, sitting at CBM $+0.51$ eV. As shown in Fig. 3, compared to the PBE calculation, GW-SOC results in shallower defect states for iodine interstitials and deeper defect states for iodine vacancies.

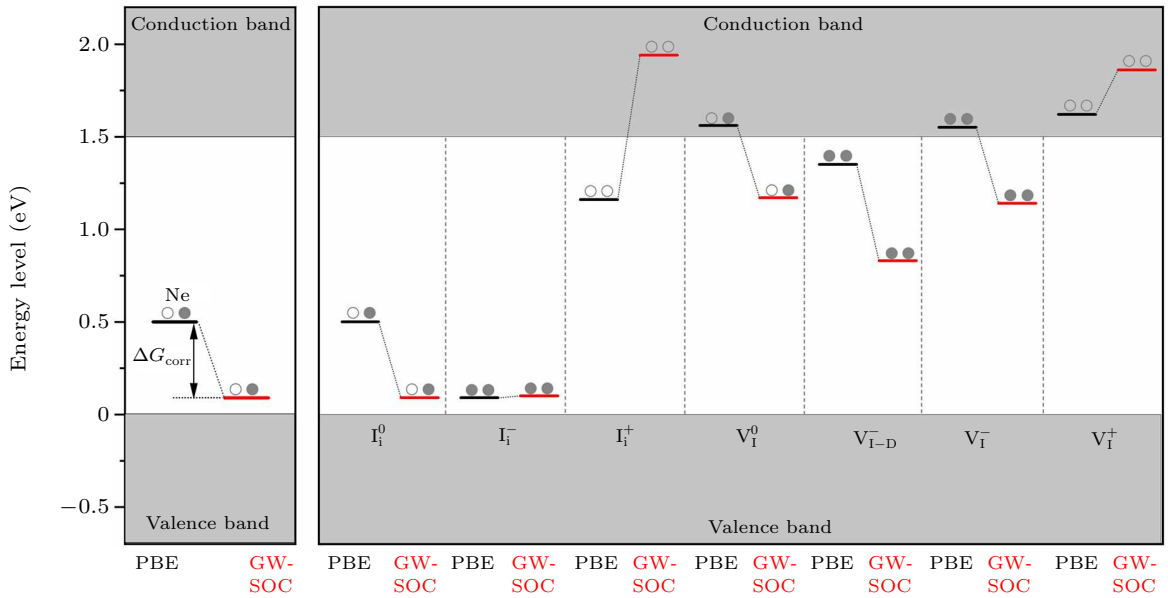

Fig. 3. Single-electron level of defective $CH_3NH_3PbI_3$ at different charge states in PBE and GW-SOC calculations. The levels are scaled to the band gap of 1.5 eV. The electronic occupancy is also shown.

3.2. GW-correction on defect calculations

Using the GW method, we recalculated $\varepsilon_D^\tau(0) - \varepsilon_{VBM}(\text{host})$ for iodine defects with different charge states and compared them with the results under a traditional PBE calculation. The difference in the single-electron level allowed us to introduce a GW correction term for correction of the single-electron level in the traditional PBE calculation as shown in Eq. (1). Taking the electronic occupancy into consideration, the defect formation energy after GW correction is accordingly obtained by the following formula:

$$\Delta H_f^{GW}(\alpha, q) = \Delta H_f^{PBE}(\alpha, q) + N_e \Delta G_{corr}, \tag{2}$$

where the GW correction term ΔG_{corr} is defined as the energy level difference between PBE and GW-SOC results and N_e is the number of electrons occupied in the defect states as shown in Fig. 3. Accordingly, the charge transition level can be calculated as

$$\varepsilon(q_1/q_2) = \frac{\Delta H_f(\alpha, q_1) - \Delta H_f(\alpha, q_2)}{q_2 - q_1}. \tag{3}$$

3.3. Multiple defect configurations

In conventional semiconductors such as Si, GaAs, and CdTe, point defects (vacancies, substitution and interstitials) are often formed in a rigid model, where the defect configurations only have little relaxations or distortions away from the original perfect crystal lattice.[35,36] However, in $CH_3NH_3PbI_3$ with a soft lattice, iodine interstitials and vacancies demonstrate multiple defect configurations, complicating defect calculations.[37] Since the local configurations directly determine the electronic and optoelectronic properties of defects, it is necessary to identify the multiple defect configurations of iodine vacancies and interstitials. It has been clarified that $CH_3NH_3PbI_3$ has both obvious ionicity and covalency.[9,30] The defect configurations can be based on a rigid model as in ionic crystals, and Pb–Pb and I–I wrong bonds can be formed as in covalent crystals.

In the conventional picture, the iodine interstitials should be an acceptor thus negatively charged, which is then favorable for bonding with positively charged Pb cations, as shown in Fig. 4(b), forming a bridge configuration where the Pb–I bonds are 3.17 Å and 3.25 Å, respectively. Those bond lengths are close to the Pb–I bond length in crystal $CH_3NH_3PbI_3$. Therefore, the bridge configuration is akin to the ionic picture, where the negatively charged I anions bond to the positively charged Pb cations. It was also found that the iodine interstitial can be positively charged and form the I–I wrong bond as in the I_3 trimer configuration shown in Fig. 4(a). In I_3 trimer configurations, the middle interstitial iodine forms a short (2.85 Å) and a long (3.71 Å) bond with neighboring I. In the neutral state, the I_3 trimer configuration is stable, but the middle I interstitial moves to the center with the short (3.56 Å) and long (3.33 Å) bond lengths being much closer to each other.

For iodine vacancies, our previous results show that it is a stable configuration, as shown in Fig. 4(d), where the iodine atom was taken out of the crystal lattice and the lattice has minimal relaxation. The nearby Pb atoms were 6.42 Å away from each other, only slightly larger than the distance in perfect crystals (6.29 Å). In the conventional picture, the iodine vacancy should be a donor thus its negatively charged states were not considered in our previous calculations. However, Agiorgousis *et al.* found that an iodine vacancy can capture one electron and form a Pb–Pb dimer configuration as shown in Fig. 4(c), where two Pb form a Pb–Pb wrong bond with a bond length of 3.35 Å, much less than their distance in a perfect crystal lattice. Such dimer configurations, as a reflection of strong covalency, were energetically favorable over the

non-dimer structure [Fig. 4(d)] by 0.67 eV in the −1 charged state. The dimer configurations are metastable in neutral and +1 charged states. The underlying mechanisms of stability on dimer and non-dimer configurations at different charged states have been discussed in our previous studies and are not extensively discussed here.

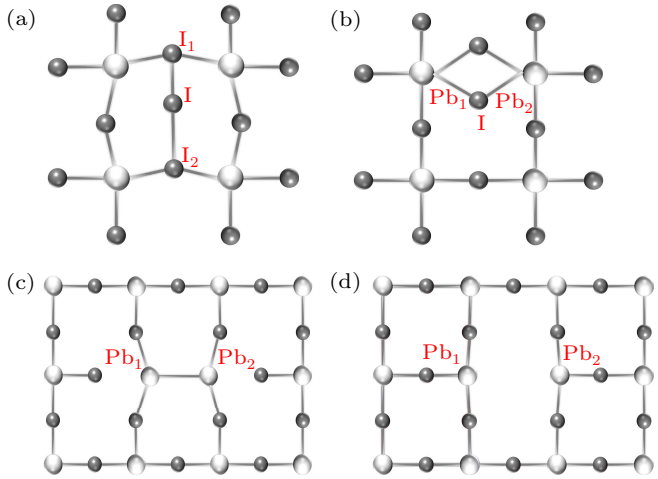

Fig. 4. (a) Crystal structure of $CH_3NH_3PbI_3$ and defective $CH_3NH_3PbI_3$ with (a) the trimer I_i, (b) the bridge I_i, (c) the dimer V_I, and (d) non-dimer V_I.

In iodine vacancies, when the dimer (non-dimer) configuration is stable in a particular charged state, the non-dimer (dimer) configuration is metastable. There is a kinetic barrier between the stable and metastable stable configurations. Likewise, in I interstitials, when the bridge (trimer) configuration is stable, trimer (bridge) configuration was found unstable.

3.4. Transition energy and formation energy

The formation energies for iodine vacancy and interstitial had been calculated using four approaches: PBE, PBE-SOC, HSE-SOC ($\alpha = 0.35$), and GW-SOC. The results are shown in Fig. 5. Defect calculations at PBE, PBE-SOC, and HSE-SOC ($\alpha = 0.35$) levels follow Eq. (1) and that at GW-SOC follows Eq. (2). Transition levels were calculated according to Eq. (3), as shown in Fig. 6. The moderate chemical potentials ($\mu_{MA} = -2.41$ eV, $\mu_{Pb} = -1.06$ eV, $\mu_I = -0.60$ eV), as the B point in Fig. 2 of Ref. [9], were chosen to show the formation energies of I_i and V_I in Fig. 5. Since the band gaps derived from each of the four approaches were different, to compare fairly, we scaled band gap and transition levels to the PBE-calculated bandgap (1.43 eV), *i.e.*, $\varepsilon = \varepsilon E_g^{PBE}/E_g^{cal}$, where ε, E_g^{PBE}, and E_g^{cal} are the transition levels, PBE calculated band gap, and band gap calculated by the other three approaches,respectively.

All four approaches concluded that neutral I_i is unstable since the stable I_i charged state is either I_i^{-1} or I_i^{+1} in the entire range of the Fermi level. The transition levels $(+1/-1)$ are 0.06, 0.04, 0.25, and 0.07 eV above the VBM in the PBE, PBE-SOC, HSE-SOC, and GW-SOC approaches, respectively. Although HSE-SOC led to a relatively deep level, all other approaches indicated that $\varepsilon(+1/-1)$ is shallow, less than 0.10 eV above the VBM, implying that the iodine interstitial may not be as detrimental as previously expected. It was previously reported in the literature that the $\varepsilon(+/0)$ for I_i is higher than its $\varepsilon(-/0)$, indicating that electron trapping at the defect leads to strong structural relaxation. The $(+/-)$ level determines the charge transition between the two stable charge states, The $(+/0)$ level is the electron trapping level for I_i^{+1}, while the $(0/-)$ level is the hole trapping level for I_i^{-1}. After calculating the related defect formation energy, it is concluded the neutral charge state of I_i is metastable. which coincides with the conclusion of this paper.[28] Similarly, Ambrosio's work pointed out that I_3 trimer is found as the most stable form of I_i^{+1} with energy levels deep in the gap of the material.[37] Note that as a donor, $\varepsilon(0/+1)$ of I_i calculated by GW-SOC is deeper than that calculated by the other three approaches, while neutral I_i is energetically unstable in equilibrium conditions. Whether it would act as strong detrimental centers under photoexcited conditions need further investigation. For V_I, four approaches gave different results as well. PBE suggested that the neutral defect is unstable and the $\varepsilon(+1/-1)$ for V_I is close to the CBM (0.26 eV below the CBM) while PBE-SOC showed that neutral V_I could be stable when the Fermi level is around the middle of band gap. This can be demonstrated in Refs. [9,34], which mentions iodine vacancies can lead to the formation of shallow trap states near the CBM and V_I^{+1} have the lowest formation energies in the lower part of Fermi level.[9,38] Moreover, the work of Agiorgousis *et al.* pointed out: When the Fermi level is higher than 1.44 eV, V_I can be stabilized at -1 charge state, otherwise, the stable charge state becomes +1, and V_I has shallow $\varepsilon(0/+)$ level but deep $\varepsilon(0/-)$, and may not be a recombination center.[30] In contrast, both HSE-SOC and GW-SOC show that −1 charged V_I is unstable and the $\varepsilon(+1/0)$ for V_I is 0.12 eV and 0.33 eV, respectively, below the CBM. These results called for a tentative investigation of the stability of V_I in the −1 charged state.

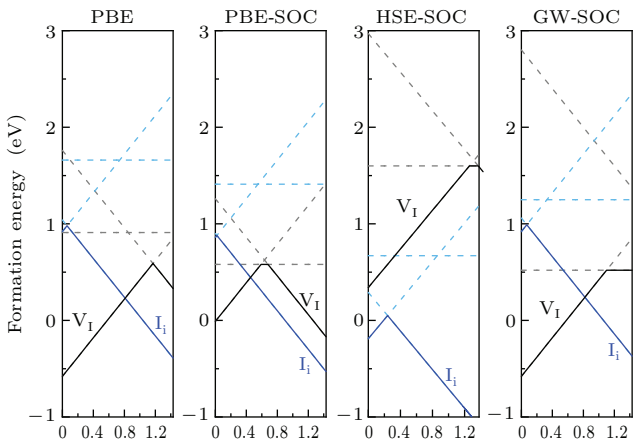

Fig. 5. Formation energies of iodine vacancies and interstitials in PBE, PBE-SOC, HSE-SOC, and GW-SOC calculations. For ease of comparison, we unified the band gap to 1.43 eV. The band gap was calculated by PBE method.

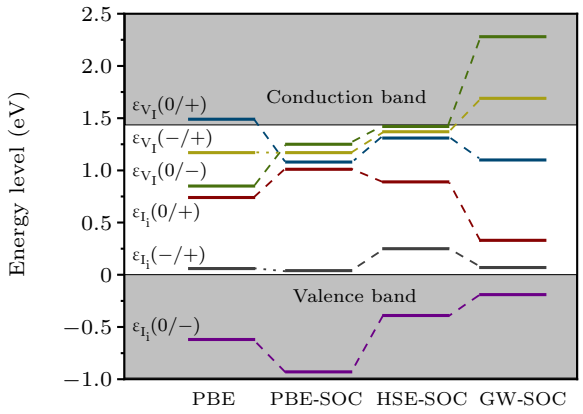

Fig. 6. Transition levels of iodine vacancies and interstitials in PBE, PBE-SOC, HSE-SOC, and GW-SOC calculations.

4. Conclusion

We developed a GW quasiparticle correction approach for calculating defects and revisited iodine vacancy and interstitial defects in $CH_3NH_3PbI_3$ as a proof of concept. The results were then compared to the results from PBE, PBE-SOC, and HSE-SOC to provide a comprehensive view of iodine defects in $CH_3NH_3PbI_3$. The results showed that GW-SOC generally pulls down the single-electron level for occupied states and pushes up the single-electron level for unoccupied states. Consistent with previous calculations, GW-SOC predicted that the neutral I interstitial was unstable and the transition level of $(+1/-1)$ was close to the VBM. Therefore, I_i may not be as detrimental as previously reported. Moreover, this study predicted that V_I may be unstable in the -1 charged state but could still be detrimental owing to the deep $(+1/0)$ transition level (0.34 eV below CBM). These results based on quasiparticle correction at the single-defect level could further facilitate the understanding of the intrinsic point defect and defect passivation observed in $CH_3NH_3PbI_3$.

Acknowledgments

Project supported by the National Natural Science Foundation of China (Grant No. 11974257), the Distinguished Young Talent Funding of Jiangsu Province, China (Grant No. BK20200003), the Priority Academic Program Development of Jiangsu Higher Education Institutions (PAPD). DFT calculations were carried out at the National Supercomputer Center in Tianjin [TianHe-1(A)].

References

[1] Buin A, Comin R, Xu J, Ip A H and Sargent E H 2015 *Chem. Mater.* **27** 4405
[2] Freysoldt C, Grabowski B, Hickel T, Neugebauer J, Kresse G, Janotti A and Van De Walle C G 2014 *Rev. Mod. Phys.* **86** 253
[3] Kang J and Wang L W 2017 *J. Phys. Chem. Lett.* **8** 489
[4] Komsa H P, Broqvist P and Pasquarello A 2010 *Phys. Rev. B* **81** 205118
[5] Oba F, Togo A, Tanaka I, Paier J and Kresse G 2008 *Phys. Rev. B* **77** 245202
[6] Hashibon A and Elsässer C 2011 *Phys. Rev. B* **84** 144117
[7] Stampfl C, Van de Walle C, Vogel D, Krüger P and Pollmann J 2000 *Phys. Rev. B* **61** R7846
[8] Sun J, Remsing R C, Zhang Y, Sun Z, Ruzsinszky A, Peng H, Yang Z, Paul A, Waghmare U, Wu X, Klein M L and Perdew J P 2016 *Nat. Chem.* **8** 831
[9] Yin W J J, Shi T and Yan Y 2014 *Appl. Phys. Lett.* **104** 063903
[10] Wang J, Li W and Yin W 2020 *Adv. Mater.* **32** 1906115
[11] Perdew J P, Burke K and Ernzerhof M 1996 *Phys. Rev. Lett.* **77** 3865
[12] Hua X, Chen X and Goddard W A 1997 *Phys. Rev. B* **55** 16103
[13] Jain A, Hautier G, Ong S P, Moore C J, Fischer C C, Persson K A and Ceder G 2011 *Phys. Rev. B* **84** 045115
[14] Kresse G and Furthmüller J 1996 *Phys. Rev. B* **54** 11169
[15] Lany S and Zunger A 2008 *Phys. Rev. B* **78** 235104
[16] Du M H 2014 *J. Mater. Chem. A* **2** 9091
[17] Kümmel S and Kronik L 2008 *Rev. Mod. Phys.* **80** 3
[18] Schonhammer K and Gunnarsson O 1987 *J. Phys. C: Solid State Phys.* **20** 3675
[19] Heyd J, Scuseria G E and Ernzerhof M 2003 *J. Chem. Phys.* **118** 8207
[20] Paier J, Marsman M and Kresse G 2007 *J. Chem. Phys.* **127** 024103
[21] Chen W and Pasquarello A 2015 *J. Phys.: Condens. Matter* **27** 133202
[22] Aryasetiawan F and Gunnarsson O 1998 *Rep. Prog. Phys.* **61** 237
[23] Yan Y and Wei S H 2008 *Phys. Status Solidi Basic Res.* **245** 641
[24] Holm B 1999 *Phys. Rev. Lett.* **83** 788
[25] Rinke P, Janotti A, Scheffler M and Van de Walle C G 2009 *Phys. Rev. Lett.* **102** 026402
[26] Ball J M and Petrozza A 2016 *Nat. Energy* **1** 16149
[27] Meggiolaro D, Motti S G, Mosconi E, Barker A J, Ball J, Andrea Riccardo Perini C, Deschler F, Petrozza A and De Angelis F 2018 *Energy Environ. Sci.* **11** 702
[28] Du M H 2015 *J. Phys. Chem. Lett.* **6** 1461
[29] Zhang X, Turiansky M E, Shen J X and Van De Walle C G 2020 *Phys. Rev. B* **101** 140101
[30] Agiorgousis M L, Sun Y Y Y, Zeng H and Zhang S 2014 *J. Am. Chem. Soc.* **136** 14570
[31] Buin A, Pietsch P, Xu J, Voznyy O, Ip A H, Comin R and Sargent E H 2014 *Nano Lett.* **14** 6281
[32] Keeble D J, Wiktor J, Pathak S K, Phillips L J, Dickmann M, Durose K, Snaith H J and Egger W 2021 *Nat. Commun.* **12** 5566
[33] Even J, Pedesseau L, Jancu J M and Katan C 2013 *J. Phys. Chem. Lett.* **4** 2999
[34] Leguy A M A, Azarhoosh P, Alonso M I, Campoy-Quiles M, Weber O J, Yao J, Bryant D, Weller M T, Nelson J, Walsh A, Van Schilfgaarde M and Barnes P R F 2016 *Nanoscale* **8** 6317
[35] Berding M A 1999 *Phys. Rev. B* **60** 8943
[36] Mattila T and Nieminen R 1996 *Phys. Rev. B* **54** 16676
[37] Ambrosio F, Mosconi E, Alasmari A A, Alasmary F A S, Meggiolaro D and De Angelis F 2020 *Chem. Mater.* **32** 6916
[38] Kye Y H, Yu C J, Jong U G G, Chen Y and Walsh A 2018 *J. Phys. Chem. Lett.* **9** 2196